

COMMUNICATION



Cite this: *J. Mater. Chem. B*, 2021, 9, 8202

Received 5th August 2021,
Accepted 9th September 2021

DOI: 10.1039/d1tb01710a

rsc.li/materials-b

Citrate-based mussel-inspired magnesium whitlockite composite adhesives augmented bone-to-tendon healing†

Xiaowei Yuan,^{‡,ab} Yitao Zhao,^{‡,b} Jintao Li,^{‡,b} Xuncaï Chen,^c Zhihui Lu,^{*b} Lianyong Li^{*a} and Jinshan Guo^{ib,*b}

Citrate-based mussel-inspired whitlockite composite adhesives (CMWAs) were developed and administered to the bone–tendon interface in anterior cruciate ligament (ACL) reconstruction. CMWAs could improve the initial bone–tendon bonding strength, promote the bony inward growth from the bone tunnel and enhance the chondrogenesis and osteogenesis of the bone–tendon interface, thus augmenting bone-to-tendon healing.

Anterior cruciate ligament (ACL) rupture is one of the most common and serious sports injuries, often leading to poor stability and dysfunction of the knee joint, secondary cartilage injury and even osteoarthritis.^{1,2} ACL reconstruction has been established as a standard ACL injury repair surgery for over 30 years, to avoid further meniscal injuries and knee replacement in the long run.³ Although conventional ACL reconstruction is able to restore partial functions of the knee joint, not all patients can fully recover moderate movement after surgery, and reinjury of the ACL happens to 30% of young active patients after returning to sports activities.⁴ One of the main reasons behind the unsatisfactory clinical outcomes is the insufficient bone-to-tendon integration and healing, especially in the early stage of ACL reconstruction.^{2,4} The bone insertion sites of the original ACL are highly specialized tissue regions with a function of pressure transfer from hard tissue to soft tissue, comprising four different types of tissue: ligaments,

uncalcified fibrocartilage, calcified fibrocartilage and bone.⁵ Studies have shown that the healing rate of the bone-to-tendon interface is much slower and more incomplete than that of bone-to-bone.^{5–11} The disordered scar tissue formation by infiltration and proliferation of a large number of fibroblasts is the main reason behind the poor healing of the bone–tendon interface.¹² Accordingly, enhancing the osteointegration of soft tissue grafts,¹³ promoting bony inward growth and tissue maturation at the interface, and inhibiting fibroblast infiltration are commonly used approaches.^{1,2} Periosteum,^{1,14} platelet rich plasma (PRP),¹⁵ mesenchymal stem cells (MSCs),¹⁶ inorganic bioactive bone cement,^{13,17} and other biomaterials have been used to modify the bone–tendon contact interface and exhibited enhanced bone-to-tendon healing performance. However, their clinical applications are still limited due to resource shortage, complex application processes, and controversial outcomes. A universal approach to improve the initial physical integration of the implanted tendon graft with the host bone tunnel and promote the following bony inward growth is highly demanded for sufficient bone-to-tendon healing.

Recently, tissue adhesives have attracted intensive research attention due to their wide applicability in soft tissue wound closure, hemostasis, leak sealing, and hard tissue fixation.^{18–24} Among the developed tissue adhesives, mussel- and tannin-inspired tissue adhesives not only can strongly adhere to soft tissue surfaces *via* the formation of covalent bonds under oxidative/alkaline conditions, but also can strongly adhere to inorganic surfaces through hydrogen bonding, surface bonding, or the formation of catechol-/gallol–metal complexes.^{19,20,24–28} This makes mussel- or tannin-inspired tissue adhesives suitable to be administered in the bone–tendon interface, and create a stable interface without fretting, by providing firm adhesion and fixation between inorganic and organic surfaces, which is believed to be beneficial for bone-to-tendon healing. By introducing mussel-inspired L-3,4-dihydroxyphenylalanine (L-DOPA) or its derivatives, such as dopamine, into citrate-based polymers, we have developed a series of injectable citrate-based

^a Department of Orthopedics; Department of Pediatric Orthopedics, Shengjing Hospital of China Medical University, Shenyang, 110004, China. E-mail: loyo_ldy@163.com; Tel: +86-24-96615-50141

^b Department of Histology and Embryology, Guangdong Provincial Key Laboratory of Construction and Detection in Tissue Engineering, School of Basic Medical Sciences; Guangdong Provincial Key Laboratory of Bone and Joint Degeneration Diseases, The Third Affiliated Hospital of Southern Medical University, Southern Medical University, Guangzhou, China. E-mail: jsguo4127@smu.edu.cn, sanlumo12@smu.edu.cn; Tel: +86-20-61648222

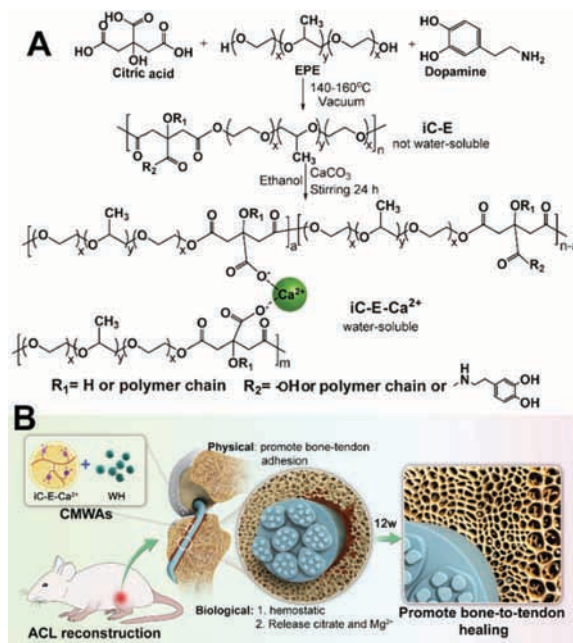
^c Department of Forensic Toxicology, School of Forensic Medicine, Southern Medical University, Guangzhou, 510515, China

† Electronic supplementary information (ESI) available. See DOI: 10.1039/d1tb01710a

‡ These authors contributed equally.

mussel-inspired bioadhesives (iCMBAs) and well demonstrated their wide applicability in both soft tissue wound closure and comminuted bone fracture adhesion.^{20,25,26,28} On the other hand, the adhesive or other materials applied on the tendon graft should be biologically supportive to the osteointegration of the tendon graft and the bony ingrowth from the host bone tunnel.¹ Citrate released during iCMA degradation could promote osteogenesis due to the high enrichment of citrate in bone (~90% of total citrate in the human body concentrated in bone), and the important biological and biomechanical functions of citrate in bone formation and bone metabolism.^{28–30} Similarly, as the fourth most common metal element in the human body,³¹ about 60% magnesium (Mg) exists in native bone and plays an important role in mineral metabolism.³² Recently, it has been found that magnesium ions could greatly promote the osteogenic differentiation of precursor cells *via* the release of a neuropeptide, calcitonin gene-related peptide (CGRP).³³ Moreover, magnesium based interference screws, as well as magnesium-pretreated periosteum, have been established to promote bone-to-tendon healing during ACL reconstruction.^{1,34,35} Magnesium-based inorganic bone cement/adhesive has also been proved to improve bone-to-tendon healing and prevent scar tissue formation in a rabbit model of ACL reconstruction.⁷ These remind us to consider a magnesium-containing mineral that naturally exists in native bone, i.e., whitlockite (WH: $\text{Ca}_{18}\text{Mg}_2(\text{HPO}_4)_2(\text{PO}_4)_{12}$), which is the second most abundant mineral after hydroxyapatite (HA), approximately 20 wt% in bone mineral, and 26–58 wt% in the mineral of teeth.³⁶ It is worth noting that the content of WH is much higher in load-bearing bone and adolescent bone, as well as in the early stage of mineralization,³⁷ indicating that it may be related to rapid bone growth and metabolism. WH is believed to release magnesium ions and transfer them into HA finally.^{36–39} The inclusion of WH to replace HA in our composite adhesive design would definitely benefit bone-to-tendon healing.

In the present work, EPE, a hydrophobic macromolecular diol was used to react with citric acid (CA) and dopamine (DP) to synthesize low swelling EPE containing iCMA prepolymer (iC-E) first, which was then treated with calcium carbonate (CaCO_3) to confer the prepolymer (iC-E- Ca^{2+}) water solubility (Scheme 1A). The introduction of calcium ions onto the side chains of the prepolymer could render it with considerable hemostatic capability,⁴⁰ beneficial to the performance of the developing adhesive as a hemostat. On the other hand, the clotted blood could localize blood-derived growth factors on the bone-tendon interface to partially replicate the functions of PRP to promote bone-to-tendon healing (Scheme 1B). Next, iC-E- Ca^{2+} was composed of 70 wt% WH, administered on the surface of a native tendon graft, and crosslinked by a frequently used oxidant, sodium periodate (PI).⁴¹ The iC-E-WH composite adhesive treated tendon graft was passed through the created bone tunnel of an ACL reconstruction model in SD rats during the adhesive crosslinking process (Scheme 1B). The effect of adhesive applied to the bone-to-tendon healing and the possible mechanisms, including the



Scheme 1 (A) Synthesis of injectable citrate-based mussel-inspired bioadhesive (iCMA, iC) prepolymers based on PEG-PPG-PEG (iC-E), which were then treated with calcium bicarbonate (CaCO_3) to give water-soluble iC-E- Ca^{2+} ; (B) the administration of citrate-based mussel-inspired magnesium whitlockite composite adhesives (CMWAs) to the bone-tendon interface in anterior cruciate ligament (ACL) reconstruction, to promote bone-to-tendon healing.

initial and long term pullout strength, bony inward growth of bone tunnel, the osteointegration and osteogenesis of the tendon graft, and fibrous scar tissue formation were thoroughly investigated. The results showed that the developed iC-E-WH composite adhesive has shown a greatly beneficial effect on bone-to-tendon healing, and thus can serve as a promising and universal auxiliary material in ACL reconstruction.

The hydrophobic iC-E prepolymer (synthesized from CA, EPE and DP according to our previous literature²⁴) was dissolved in ethanol, then reacted with an excess amount of CaCO_3 to introduce calcium ions onto the side carboxyl groups of iC-E, to give water soluble iC-E- Ca^{2+} prepolymer after dialysis and freeze-drying (Scheme 1A). The FTIR spectra of iC-E- Ca^{2+} and iC-P (synthesized using PEG_{200} , instead of EPE, for comparison) are shown in Fig. 1A. The peak between 1700 and 1748 cm^{-1} was assigned to the carbonyl bond ($\text{C}=\text{O}$) in the ester group. The peak at 1540 cm^{-1} was assigned to the amide group ($-\text{C}(=\text{O})-\text{NH}-$), confirming the formation of amide linkages between the $-\text{COOH}$ groups of CA and the $-\text{NH}_2$ groups of DP. The peaks around 2932 and 2870 cm^{-1} for iC-E- Ca^{2+} were much stronger than that of iC-P, which were assigned to the methyl ($-\text{CH}_3$) and methylene ($-\text{CH}_2-$) groups from EPE. The ^1H NMR spectra of iC-E- Ca^{2+} and iC-P are shown in Fig. 1B. The characteristic peaks of catechol groups at 6.40–6.70 ppm showed up in the spectra of both iC-E- Ca^{2+} and iC-P prepolymers, confirming the successful introduction of DP. While the peak at 1.02 ppm in the spectrum of iC-E- Ca^{2+} was assigned to

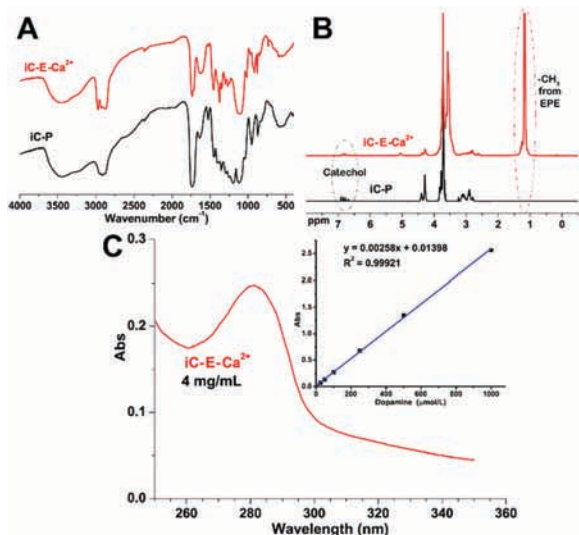


Fig. 1 Characterization of prepolymers: (A) FTIR, (B) ^1H -NMR of iC-E- Ca^{2+} and iC-P (iCMBAs composed of citric acid, poly(ethylene glycol) with a molecular weight of 200 Da (PEG₂₀₀), and dopamine); (C) UV-vis absorption spectrum of iC-E- Ca^{2+} (0.4 mg mL^{-1}) in aqueous solution. The insert panel in C is the standard curve of dopamine in aqueous solution.

the protons of $-\text{CH}_3$ from EPE, which was not present in the ^1H NMR spectrum of iC-P. The FTIR and ^1H NMR results confirmed the esterification reaction between CA and EPE, and the formation of amide linkages between the $-\text{COOH}$ groups of CA and $-\text{NH}_2$ groups of dopamine. The availability of catechol hydroxyl groups in iC-E- Ca^{2+} prepolymer was further verified *via* the UV absorption peak at 280 nm (Fig. 1C). And the content of the catechol group in the iC-E- Ca^{2+} prepolymer was determined to be $0.241 \text{ mmol g}^{-1}$, according to the dopamine standard curve shown in the inset panel in Fig. 1C.

The gel times of iC-E- Ca^{2+} prepolymer solution crosslinked by different concentrations of PI are shown in Table 1 and Fig. 2A. For 33.3 wt% iC-E- Ca^{2+} prepolymer solution without mixing inorganic substances, the gel time ($196 \pm 39 \text{ s}$) was the shortest when the concentration of PI was 1 wt% (Table 1 and Fig. 2A). The gel time further decreased to $143 \pm 12 \text{ s}$ after adding 70 wt% WH (to the total dry weight of prepolymer and

Table 1 Gel times of 33 wt% iC-E- Ca^{2+} solution and its composite with whitlockite (WH) crosslinked by sodium periodate (PI) solutions with different concentrations, and the nomenclature of crosslinked hydrogels

Prepolymer name	PI concentration ^a (wt%)	Gel time ^b (s)	Name of crosslinked hydrogel
iC-E- Ca^{2+}	1	196 ± 39	iC-E-1PI
iC-E- Ca^{2+}	2	219 ± 16	iC-E-2PI
iC-E- Ca^{2+}	3	564 ± 12	iC-E-3PI
iC-E- Ca^{2+}	4	794 ± 31	iC-E-4PI
iC-E- Ca^{2+}	8	945 ± 13	iC-E-8PI
iC-E- Ca^{2+} /70wt% WH	2	143 ± 12	iC-E-70WH ^c

^a The volume ratio between PI solution and prepolymer solution was kept as 2 : 1 for all samples. ^b The testing temperature was $25 \text{ }^\circ\text{C}$ for all samples. ^c For all composite hydrogels containing WH, 2 wt% PI solution was used as the crosslinking initiator.

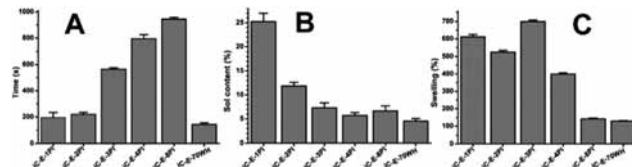


Fig. 2 Crosslinking of prepolymers: (A) gel times (obtained by tilting tests), (B) sol contents, and (C) swelling ratios of iC-E- Ca^{2+} prepolymer and its composite with whitlockite ($\text{Ca}_{18}\text{Mg}_2(\text{HPO}_4)_2(\text{PO}_4)_{12}$). WH crosslinked by sodium periodate (PI) with different concentrations.

WH) to iC-E- Ca^{2+} prepolymer solution. It is strange that with the increase of PI concentration, the gel times became even longer. The gel time of pure 33.3 wt% iC-E- Ca^{2+} prepolymer solution crosslinked by 8 wt% PI reached $945 \pm 13 \text{ s}$ (Fig. 2A). We believe that the calcium ions on the side chains of the iC-E- Ca^{2+} prepolymer may react with PI to reduce its water solubility, thus prolonging the catechol oxidation and the crosslinking processes. Since one calcium ion could react with two periodate ions, a precipitation complex might not be formed at lower PI concentrations.

Sol contents of iC-E- Ca^{2+} and its composite with WH crosslinked by different concentrations are shown in Fig. 2B. The sol contents of all the tested formulas were lower than 30%, with the sol content of iC-E-1PI the highest ($25.2 \pm 3.5\%$). The increase of PI concentration led to decreased sol content, indicating that higher PI concentration induced higher crosslinking density. The iC-E-70WH (crosslinked by 2 wt% PI) possessed the lowest sol content ($<5\%$). The increase of PI concentration also led to a lower swelling ratio, and the swelling ratio of iC-E-8PI ($\sim 120 \text{ wt}\%$) was much lower than that of iC-E-1PI, iC-E-2PI, iC-E-3PI and iC-E-4PI (all higher than 400 wt%), further confirming that iC-E-8PI possessed higher crosslinking density (Fig. 2C). The swelling ratio of iC-E-70WH was also the lowest ($\sim 100 \text{ wt}\%$) in the tested formula (Fig. 2C).

The mechanical properties of crosslinked iC-E- Ca^{2+} adhesives in dry and 10% hydrated states are tabulated in Table 2 and represented in Fig. 3A–D. From Fig. 3A, it can be seen that the tensile strengths were improved from $1.28 \pm 0.15 \text{ MPa}$ for iC-E-2PI to $3.33 \pm 0.52 \text{ MPa}$ for iC-E-70WH after compositing WH in the adhesives. The Young's moduli greatly improved from $2.66 \pm 0.24 \text{ MPa}$ for iC-E-2PI to $62.03 \pm 8.60 \text{ MPa}$ for iC-E-70WH (Fig. 3B). While along with the increase of WH content in the composite, the elongation at break quickly dropped from $428.47 \pm 73.48\%$ for iC-E-2PI to $6.72 \pm 1.50\%$ for iC-E-70WH (Fig. 3C), the trend could also be seen from the stress–strain curves of the crosslinked dry composite adhesives shown in Fig. 3D. The tensile strength of iC-E-70WH decreased from $3.33 \pm 0.19 \text{ MPa}$ for a dry sample to $1.95 \pm 0.59 \text{ MPa}$ for a hydrated sample after absorbing 10 wt% (to its dry weight) water (Table 2). The mechanical strengths of other samples also decreased at a hydrated state (Table 2).

The degradation profiles of the crosslinked composite adhesives are shown in Fig. 3E and 3F. The degradation of iC-E-2PI (with $\sim 90\%$ mass loss after 63 days) was much slower than that of PEG-based iCMBAs (full degradation could be reached in

Table 2 Mechanical properties of different crosslinked hydrogels, in dry and 10 wt% hydrated (swollen) states

Crosslinked hydrogel ^a	Tensile strength (MPa)		Young's modulus (MPa)		Elongation at break (%)	
	Dry	Swollen	Dry	Swollen	Dry	Swollen
iC-E-2PI	1.28 ± 0.05	0.26 ± 0.09	2.66 ± 0.08	2.58 ± 0.27	428.47 ± 25.98	294.97 ± 87.47
iC-E-30WH ^b	2.47 ± 0.04	1.31 ± 0.19	8.52 ± 0.48	8.61 ± 1.54	252.26 ± 18.7	287.71 ± 60.21
iC-E-50WH ^b	3.1 ± 0.16	2.38 ± 0.45	26.88 ± 1.03	27.35 ± 3.07	32.29 ± 2.53	204.56 ± 46.83
iC-E-70WH ^b	3.33 ± 0.19	1.95 ± 0.59	62.03 ± 3.04	63.36 ± 8.90	6.72 ± 0.53	5.52 ± 1.96

^a The concentration of PI solution was 2 wt%. ^b 30, 50, and 70 represents the percentage of WH in the dry weight of prepolymer and WH.

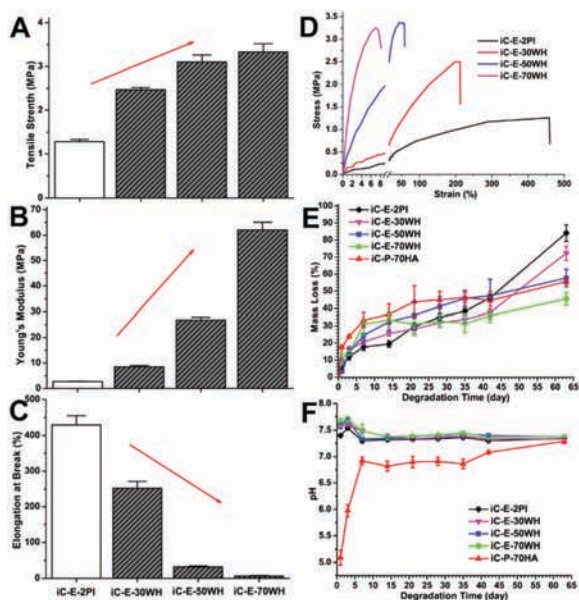


Fig. 3 Mechanical properties and degradation profiles: (A) tensile strength, (B) Young's modulus, (C) elongation at break, and (D) stress-strain curves of air-dried iC-E-2PI and iC-E-30/50/70WH samples; (E) degradation profiles and (F) pH change of the buffer solutions during the degradation of iC-E-2PI, iC-E-30/50/70WH and iC-P-70HA in PBS (pH 7.4) at 37 °C.

30 days) previously developed in our group^{19,20,25} (Fig. 3E). This may be attributed to the hydrophobicity of EPE and the introduction of additional ion crosslinking between the calcium ions and the ionized carboxyl groups on the side chains of iC-E-Ca²⁺. The inclusion of HA or WH further prolonged the degradation time. After 63 days of degradation, the mass loss of iC-E-70WH was less than 50% (45.39 ± 3.74%) (Fig. 3E). The degradation of iC-P-70HA is relatively faster than that of iC-E-70WH. At the same time, the pH values of the degradation solutions of different samples were also measured and analyzed, and the results are shown in Fig. 3F. It can be seen that the pH values of the degradation solutions of iC-E-2PI, iC-E-30WH, iC-E-50WH and iC-E-70WH fluctuated within pH 7.7 to 7.3 in the initial week of degradation, and stabilized in the range of 7.3 to 7.4 over the next six weeks. While the pH value of the initial degradation solution of iC-P-70HA at day 1 was 5.1 ± 0.1, showing it to be much lower than all iC-E-Ca²⁺ adhesive samples, also indicating that the treatment of iC-E with CaCO₃ greatly neutralized the acidity of the prepolymer. The pH values of iC-P-70HA degradation solutions slowly

increased with the extension of degradation time, and finally reached pH 7.3 after 63 days, further proving the benefit of CaCO₃ treatment for the biocompatibility of the composite adhesives (Fig. 3F).

WH could release magnesium ions and transfer them into HA finally, and thus it is considered as the precursor of HA.^{36–38} The release of magnesium and calcium ions from the cross-linked composite adhesives was studied, the results are shown in Fig. 4A and B. It can be seen that iC-E-70WH exhibited prolonged magnesium and calcium ion release at high concentrations, while the metal ion release from iC-E-30WH and iC-E-50WH slowed down after 2 weeks. The metal ion concentrations in the released solution were in the range of 10–40 ppb (parts per billion) for both magnesium and calcium ions in all three samples. Note that both WH and iC-E-Ca²⁺ prepolymer can release calcium ions. These results proved the magnesium and calcium ions long term release capability of the composite adhesives, which is beneficial to the improvement of the bioactivity.

The cell cytotoxicity of magnesium ions in different concentrations was assessed against rBMSCs using the CCK-8 assay. As shown in Fig. 4C, 100 mmol L⁻¹ Mg²⁺ induced significant toxicity against rBMSCs with a cell viability of less than 5%. While, the cell viabilities of Mg²⁺ with concentrations lower

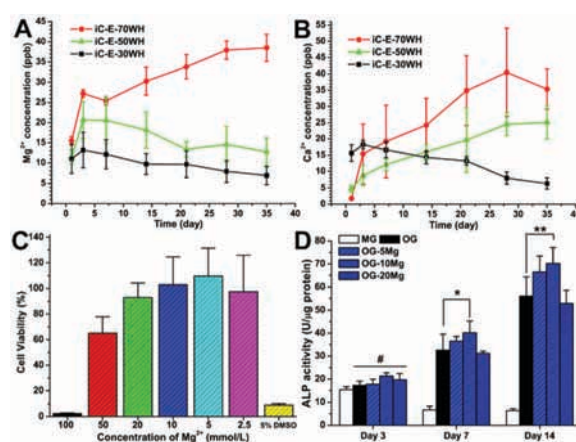


Fig. 4 Metal ion release profiles, cytotoxicity and alkaline phosphatase (ALP) activity of magnesium: the release profiles of (A) magnesium and (B) calcium ions from cross-linked iC-E-30/50/70WH in PBS (pH 7.4) solution at 37 °C; (C) cytotoxicity of magnesium ions against BMSCs; (D) the effect of magnesium ions in 5 (OG-5Mg), 10 (OG-10Mg) or 20 (OG-20Mg) mmol L⁻¹ to the ALP activity during osteogenic differentiation of BMSCs. # *p* > 0.05, * *p* < 0.05, ** *p* < 0.01.

than 50 mmol L⁻¹ were all higher than 60%, indicating suitable cytocompatibility of Mg²⁺ at concentrations lower than 50 mmol L⁻¹ (Fig. 4C). The strong toxicity of 5% DMSO proved the reliability of this cell cytocompatibility study (Fig. 4C). The effect of magnesium ions on the osteogenic differentiation of rBMSCs was also studied using ALP assay. When rBMSCs showed osteogenic differentiation induced by osteogenic media, after including Mg²⁺ of 5, 10 or 20 mmol L⁻¹ (following in the cytocompatible level), the ALP activities were improved 3–9 fold at days 7 and 14, indicating the strong osteoinductivity of Mg²⁺ (Fig. 4D). Mg²⁺ with concentrations of 5 and 10 mmol L⁻¹ induced the highest ALP expression, a further increase in the Mg²⁺ concentration caused a decline of ALP expression (Fig. 4D).

The cell cytotoxicity results of iC-E-Ca²⁺ and iC-P prepolymers against rBMSCs are shown in Fig. 5A. At 10 mg mL⁻¹, although the cell viability of iC-E-Ca²⁺ (<10%) was lower than that of iC-P, it was comparable to that of PEGDA. In diluted iC-E-Ca²⁺ prepolymer solutions of 1 and 0.1 mg mL⁻¹, the cell viabilities were similar to or higher than that of blank medium or PEGDA, indicating the low cytotoxicity of the prepolymers. The cell viabilities of the soluble substances of crosslinked iC-E-XPI (X = 1, 2, 3, 4, and 8) at 1× concentration were all around 10%, and the inclusion of 70 wt% WH increased the cell viability to around 30% (Fig. 5A). Meanwhile, the cell viabilities

of soluble substances at 10× and 100× dilutions were all around 80% (Fig. 5B). However, for the degradation products 1× degradation solutions of iC-E-XPI all exhibited higher cytotoxicities (cell viabilities ~20%) compared to that of iC-E-70WH and PLGA (~80%) (Fig. 5C). The diluted degradation product solutions of iC-E-Ca²⁺ based adhesives at 10× and 100× were all higher than 90% except for iC-E-1PI, and comparable to that of the PLGA degradation solution at the same dilutions (Fig. 5C), further confirming the cytocompatibility of the crosslinked composite adhesives.

The effect of CMWAs on the proliferation and differentiation of rBMSCs was investigated using the ALP assay (Fig. 5D), live/dead and ARS staining (Fig. 5E). rBMSCs were cultured in growth media (MG), osteogenic media (OG) and OG with the degradation products of iC-E-2PI (OiC), iC-E-70WH (OiCW70) or iC-P-70HA (OiC₂₀₀H70). The OiCW70 was also filtered to give OiCW media, to investigate the effect of WH. As shown in Fig. 5D, at day 3, no significant difference can be observed between all the tested groups. However, on days 7 and 14, the ALP expression levels of the OiC₂₀₀H70 and OiCW70 groups were all significantly higher than that of the OG group at the same time points. The ALP expression of OiCW70 was also significantly higher than that of OiC₂₀₀H70; in particular, at day 14 (*p* < 0.05). These results indicate the positive effect of citrate-based adhesive and WH in rBMSCs' osteogenic differentiation and the superior bioactivity of WH compared to HA. From the Live/Dead images (Fig. 5E, left panel), it can be seen that rBMSCs grew well for all five groups. The cell densities increased along with time and reached confluence after 14 days. The stretched cell morphology of rBMSCs indicated good cell attachment and proliferation co-cultured with the degradation products of crosslinked composite adhesives. The calcium deposit formation of rBMSCs after osteogenic differentiation was also assessed using ARS staining (Fig. 5E, right panel). It can be seen that no calcium deposits were found in the MG group at all time-points. In the OG group, only a small amount of calcium deposits could be observed after 14 days, less than that in the OiC, OiCW and OiCW70 groups. On day 21, the calcium deposits in the OiC, OiCW and OiCW70 groups were significantly higher than that of the OG group, and the OiCW70 group had the highest amount of calcium deposits (Fig. 5E, right panel). It is worth mentioning that, the inclusion of WH and citrate-based adhesive not only induced more calcium deposits, but also earlier calcium deposition (Fig. 5E, right panel), further confirming the bioactivity of citrate and WH in the osteogenic differentiation and mineralization of rBMSCs.

The hemostatic performance of the iC-E-Ca²⁺ prepolymer and its composite adhesive with WH was assessed with a standardized strip rat liver blood clotting method. From Fig. 6A and B, it can be seen that without the CaCO₃ treatment, the blood clotting time of the iC-E group was much longer than that of the control group, which is attributed to the anticoagulant property of citrate. Sodium citrate is a well-known clinically used anticoagulant. While the CaCO₃ treatment confers considerable hemostatic capability to thus-obtained

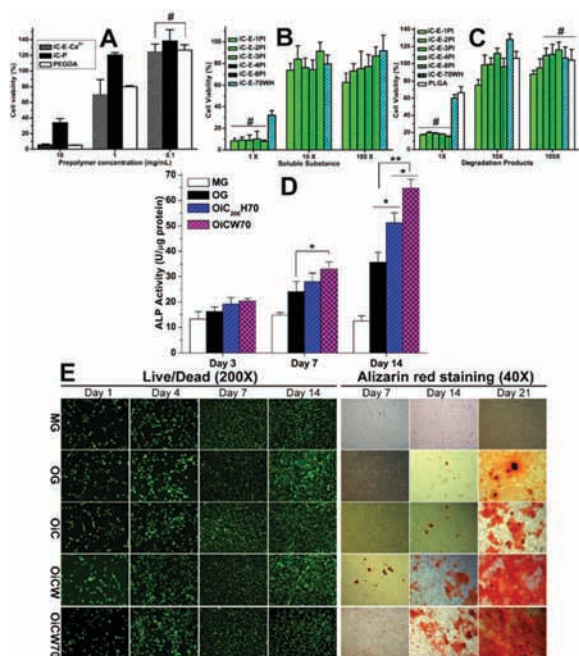


Fig. 5 Cytocompatibility and osteogenic differentiation evaluation: cytotoxicity of iC-E-Ca²⁺ composite adhesives against rat bone mesenchymal stem cells (rBMSCs) through the CCK-8 assay for (A) prepolymers, (B) soluble substances (sol content) and (C) degradation products; (D) ALP activity of osteogenic differentiated rBMSC cocultured with iC-E-70WH (OiCW70) and iC-P-70HA (OiC₂₀₀H70) degradation products; (E) live/dead and alizarin red staining of rBMSC treated with growth media (MG), osteogenic media (OG), osteogenic media with degradation products of iC-E-2PI (OiC), iC-E-70WH (filtered, OiCW), and iC-E-70WH (unfiltered, OiCW70). #*p* > 0.05, **p* < 0.05, ***p* < 0.01.

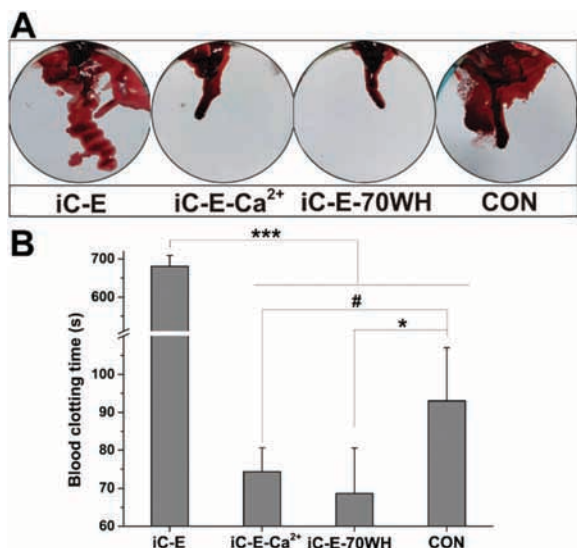


Fig. 6 (A) Photos of blood loss and (B) blood clotting times of iC-E, iC-E-Ca²⁺ prepolymers and the composite adhesive iC-E-70WH derived by a standardized strip rat liver injury blood clotting test. #*p* > 0.05, **p* < 0.05, ****p* < 0.001.

iC-E-Ca²⁺ prepolymer, the blood clotting time of the iC-E-Ca²⁺ sample was vastly shortened to ~75 s from ~700 s for the iC-E group, and became shorter than that of the control group (no significant difference) (Fig. 6B). The inclusion of WH further reduced the blood clotting time, and the iC-E-70WH group showed the shortest blood clotting time of less than 70 s. At the same time, the iC-E-Ca²⁺ and iC-E-70WH samples induced much less blood loss compared to that in the iC-E and control groups, reflecting much smaller blood contaminated areas of the two calcium ion containing groups (Fig. 6A). The hemostatic ability of the iC-E-Ca²⁺ prepolymer and its composites induces less blood loss and immobilizes the blood clots on the surface of the implanted tendon, to partially replicate the function of platelet rich plasma (PRP), to promote bone-to-tendon healing.

To assess the *in vivo* biocompatibility and bone-to-tendon regeneration performance of CMWAs, and to investigate the effect of WH, iC-E-70WH was chosen as a representative tissue adhesive to wrap on the surface of the autologous tendon which was then used in the ACL reconstruction model on SD rats. The bone adhesive (iC-P-70HA) prepared according to our previous literature²⁸ was used as the positive control, iC-E-2PI without WH and untreated ACL capture were used as negative controls. At 4, 8, and 12 weeks post ACL reconstruction, the reconstructed ACL and the surrounding tissues were harvested, and biomechanical tests, micro-computer tomography (micro-CT) analysis, and histological examination were conducted.

To investigate the effect of adhesive application on the initial bone-to-tendon bonding strength, as well as the long term osteo-integration of the implanted tendon, biomechanical strength tests (Fig. 7A) were conducted 4 and 12 weeks after the ACL reconstruction. As shown in Fig. 7B, it can be seen that at week 4, the pull-out forces for the three adhesive groups were

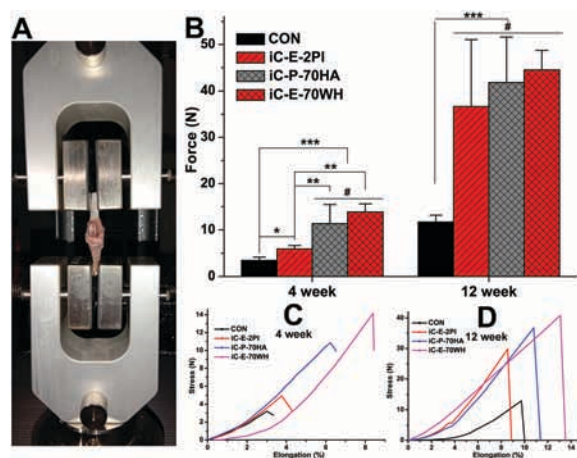


Fig. 7 Biomechanical test results: (A) representative femur-graft-tibia complex biomechanical test set-up; (B) the tested pullout forces of the femur-graft-tibia complexes treated with different samples 4 and 12 weeks post ACL reconstruction. The representative stress-elongation curves of different samples at (C) week 4 and (D) week 12. #*p* > 0.05, **p* < 0.05, ***p* < 0.01, ****p* < 0.001.

all significantly higher than that of the control group. The pull-out forces of HA or WH containing adhesive groups were also significantly higher than that of the iC-E-2PI group (Fig. 7B and C). After 12 weeks, the pull-out forces for the three adhesive groups further enhanced, they were all 2–3 times higher than that of the control group (*p* < 0.001) (Fig. 7B and D). There were no significant differences in the pull-out forces between the three adhesive groups at week 12. These results confirmed that the application of tissue adhesives especially WH and HA containing composite adhesives could greatly improve the initial bone-to-tendon bonding strength and the osteointegration of the implanted tendon, to promote bone-to-tendon healing.

From the 3D images reconstructed by micro-CT analysis shown in Fig. 8A, it can be seen that all the sizes of the bone tunnels treated with different samples decreased over time, including the control (CON) group. There is no significant difference between the iC-E-2PI group and the CON group. While, both iC-P-70HA and iC-E-70WH induced faster size decrease than that of the CON and iC-E-2PI groups, confirming that the inclusion of CMWAs in ACL reconstruction could promote the bony inward growth from the bone tunnel. This was also confirmed through the quantitative BV/TV (Fig. 8B) and BMD (Fig. 8C) data, in which that the BV/TV and BMD values of the iC-E-70WH group at nearly all the three time-points were significantly higher than that of the other three groups including the iC-P-70HA group (Fig. 8B and C). The iC-E-70WH group possessed the maximum bone tunnel size decrease and new bone formation, indicating the superior osteoconductivity and osteoinductivity of WH than that of HA (Fig. 8). The long-term release of Mg²⁺ (from WH) and Ca²⁺ (from both WH and iC-E-Ca²⁺) from iC-E-70WH was considered to contribute to the superior osteogenic activity of iC-E-70WH tissue adhesive in bone-to-tendon healing.

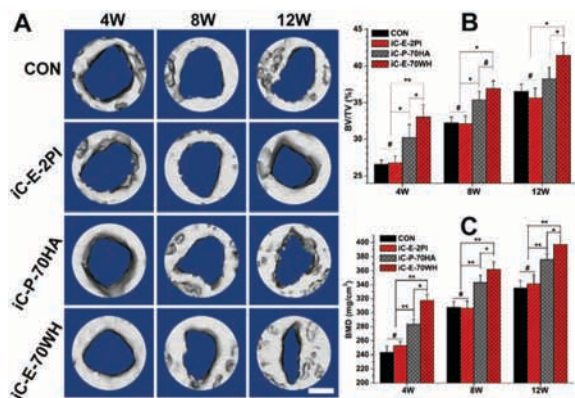


Fig. 8 Micro-CT analysis results: (A) representative 3D images of transverse slices derived from micro-CT analysis of the volume of interest (VOI) 4, 8, and 12 weeks after ACL reconstruction (the original size of the bone tunnel was 1.5 mm in diameter), scale bar = 0.5 mm; the (B) bone volume/total volume fractions (BV/TVs) and (C) bone mineral densities (BMDs) in the VOIs of different samples at different time-points calculated by micro-CT. # $p > 0.05$, * $p < 0.05$, ** $p < 0.01$.

After 4, 8 and 12 weeks post ACL reconstruction surgery, the bone–tendon interface as well as the host bone tunnel tissues were harvested and investigated by H&E and Masson’s trichrome staining. At week 4, some messy fibrous tissue can be found in the bone–tendon interface in the control (CON) group, which was rarely seen in the adhesive (iC-E-2PI, iC-P-70HA and iC-E-70WH) groups, indicating that the application of adhesive was conducive to the orderly growth of bone marrow

mesenchymal stem cells and could eliminate the infiltration of fibroblasts, thus reducing the formation of scar tissue (Fig. 9A–C). As shown in Fig. 9A and B, an obvious gap existed in the bone–tendon interface for all samples at week 4, which could also be clearly seen in the large-area staining images shown in Fig. 9C. These gaps became smaller at week 8, and there was nearly no gap at the bone–tendon interface at week 12, especially for adhesive treated groups (Fig. 9A and B). At week 12, some cartilage tissues showed up in the bone–tendon interface in all groups (labelled as “C” in Fig. 9A and B), and more calcified fibrocartilage could be observed in the iC-E-70WH group compared with iC-P-70HA and other groups, suggesting that the inclusion of a mineral component, especially Mg^{2+} releasing WH, could promote ossification, beneficial to the rapid bony inward growth and bone-to-tendon healing.

To further investigate the effect of CMWAs on the chondrogenesis and osteogenesis of the bone-to-tendon interface, collagen 2 (COL2, cartilage marker) and Runt-related transcription factor 2 (Runx2) immunohistochemical staining of the bone–tendon interface tissue sections and corresponding quantitative analysis was conducted. From Fig. 9D and F, it can be seen that, at week 4, the COL2 expression levels of the iC-P-70HA and iC-E-70WH groups were significantly higher than that of the CON and iC-E-2PI groups at week 4 ($p < 0.01$). While the COL2 expression of the composite adhesive groups (iC-P-70HA and iC-E-70WH) showed a downward trend along with the increase in time. At the same time, the COL2 expression levels of the

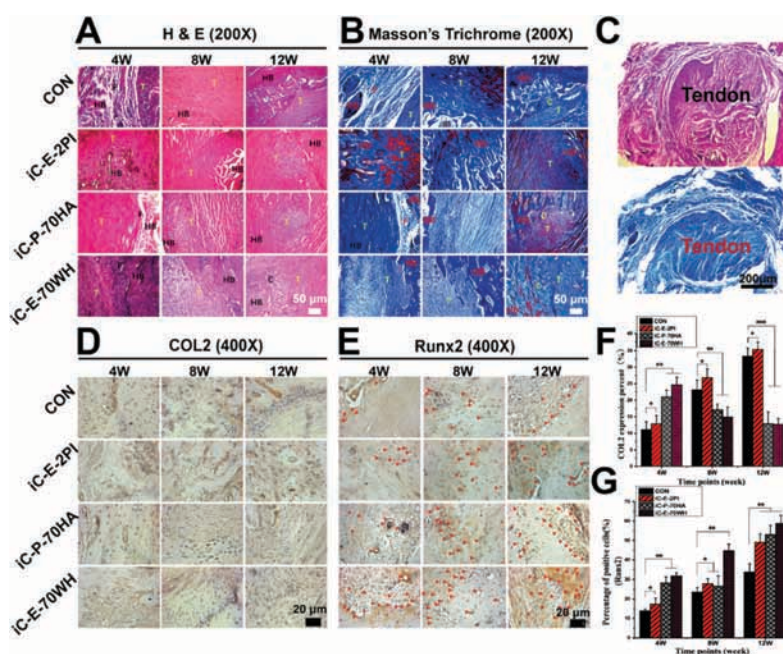


Fig. 9 Histological examination results. (A, top panel of C) H & E (hematoxylin and eosin) and (B, low panel of C) Masson’s trichrome staining images of the reconstructed ACL and the surrounding tissue sections for iC-E-2PI, iC-P-70HA, iC-E-70WH and the blank control (CON) 4, 8 and 12 weeks after the operation (T: tendon, HB: host bone, F: fibrous tissue, C: cartilage). (D) COL2 (collagen 2) and (E) Runx2 (Runt-related transcription factor 2) immunohistochemical staining images; (F) COL2 (COL2 positive areas are labeled as blue color triangles) expression percents (%) and (G) percentages of Runx2 positive cells (labeled by red color triangles) reflecting the osteogenesis and chondrogenesis during ACL reconstruction. * $p < 0.05$, ** $p < 0.01$, *** $p < 0.001$.

CON and iC-E-2PI groups increased with time and became significantly higher than that of the two composite adhesive groups at weeks 8 and 12 (Fig. 9D and F). In contrast, the Runx2 secretion of the iC-P-70HA and iC-E-70WH groups kept an increasing trend and maintained higher levels than that of the CON and iC-E-2PI groups at all three tested time points (Fig. 9E and G). These results suggested that in the iC-P-70WH group, the endochondral osteogenesis was accelerated, which is beneficial to the initial stabilization of the bio-environment of the bone–tendon interface and the acceleration of bone-to-tendon healing.

In conclusion, by treating hydrophobic poly(ethylene glycol)-*block*-poly(propylene glycol)-*block*-poly(ethylene glycol) (EPE) containing injectable citrate-based mussel-inspired bioadhesive (iCMBA) prepolymer (iC-E) with calcium carbonate (CaCO₃), a water-soluble and hemostatic prepolymer iC-E-Ca²⁺ was synthesized. Then, iC-E-Ca²⁺ was composited with a natural magnesium containing mineral, whitlockite (WH, Ca₁₈Mg₂(HPO₄)₂(PO₄)₁₂), and crosslinked with sodium periodate (PI) to develop citrate-based mussel-inspired WH composite adhesives (CMWAs) as an adhesive used in the bone–tendon interface in ACL reconstruction. CMWAs exhibited high gelation speeds, low swelling ratios, considerable mechanical strengths and tunable degradation profiles. Benefitting from both citrate-based adhesive prepolymer and WH, the CMWAs, such as iC-E-70WH, demonstrated excellent *in vitro* and *in vivo* biocompatibility, favorable hemostatic ability, osteoconductivity and osteoinductivity. The CMWAs administered in the bone–tendon interface could improve both the physical and biological environment of the reconstructed ACL. The CMWAs stabilized the initial physical environment by providing considerable adhesion between the inorganic surface of the host bone and the organic surface of the implanted tendon, enhanced long-term osteointegration of the implanted tendon, stopped bleeding to localize blood derived growth factors, and promoted the bony inward growth of the bone tunnel as well as the chondrogenesis and osteogenesis of the bone–tendon interface, thus accelerating bone-to-tendon healing in ACL reconstruction. The developed CMWAs could serve as a promising and universal auxiliary material to promote bone-to-tendon healing in ACL reconstruction, and greatly expanded the application of tissue adhesives.

Author contributions

Xiaowei Yuan: experiment conduction, data production, manuscript draft; Yitao Zhao: histological examination, hemostatic experiment; Jintao Li: ICP-MS tests; Xuncai Chen: direction on ICP-MS tests; Zhihui Lu: revision; Lianyong Li: supervision; Jinshan Guo: conception, supervision, writing, revision.

Conflicts of interest

There are no conflicts to declare.

Acknowledgements

We are thankful for the support from the Biomaterial Research Center, School of Biomedical Engineering of Southern Medical University. The project was supported by the National Natural Science Foundation of China (NSFC, No. 82102545) and the Joint Foundation for Basic and Applied Basic Research Project of Guangdong Province (20201910240000115).

Notes and references

- 1 J. Wang, J. Xu, X. Wang, L. Sheng, L. Zheng, B. Song, G. Wu, R. Zhang, H. Yao, N. Zheng, M. T. Yun Ong, P. S. Yung and L. Qin, *Biomaterials*, 2021, **268**, 120576.
- 2 P. Y. Mengsteab, T. Otsuka, A. McClinton, N. S. Shemshaki, S. Shah, H. M. Kan, E. Obopilwe, A. T. Vella, L. S. Nair and C. T. Laurencin, *Proc. Natl. Acad. Sci. U. S. A.*, 2020, **117**, 28655–28666.
- 3 H. S. Kim, J. K. Seon and A. R. Jo, *Knee Surg. Relat. Res.*, 2013, **25**, 165–173.
- 4 M. V. Paterno, M. J. Rauh, L. C. Schmitt, K. R. Ford and T. E. Hewett, *Am. J. Sports Med.*, 2014, **42**, 1567–1573.
- 5 X. Tian, Z. Lu, C. Ma, M. Wu, C. Zhang, Y. Yuan, X. Yuan, D. Xie, C. Liu and J. Guo, *Mater. Sci. Eng., C*, 2021, **121**, 111807.
- 6 L. Cui, J. Zhang, J. Zou, X. Yang, H. Guo, H. Tian, P. Zhang, Y. Wang, N. Zhang, X. Zhuang, Z. Li and J. Ding, *Biomaterials*, 2020, **230**, 119617.
- 7 L. V. Gulotta, D. Kovacevic, L. Ying, J. R. Ehteshami, S. Montgomery and S. A. Rodeo, *Am. J. Sports Med.*, 2008, **36**, 1290–1297.
- 8 D. Zhao, T. Zhu, J. Li, L. Cui, Z. Zhang, X. Zhuang and J. Ding, *Bioact. Mater.*, 2020, **6**, 346–360.
- 9 T. Zhu, Y. Cui, M. Zhang, D. Zhao, G. Liu and J. Ding, *Bioact. Mater.*, 2020, **5**, 584–601.
- 10 Y. Zhang, X. Liu, L. Zeng, J. Zhang, J. Zuo, J. Ding and X. Chen, *Adv. Funct. Mater.*, 2019, **29**, 1903279.
- 11 D. Zhao, T. Zhu, J. Li, L. Cui, Z. Zhang, X. Zhuang and J. Ding, *Bioact. Mater.*, 2021, **6**, 346–360.
- 12 M. Golman, X. Li, D. Skouteris, A. A. Abraham, L. Song, Y. Abu-Amer and S. Thomopoulos, *Am. J. Sports Med.*, 2021, **49**, 780–789.
- 13 G. M. Kuang, W. P. Yau, W. W. Lu and K. Y. Chiu, *Sports Traumatol. Arthrosc.*, 2010, **18**, 1038–1051.
- 14 H. S. Kyung, S. Y. Kim, C. W. Oh and S. J. Kim, *Knee Surg. Sports Traumatol. Arthrosc.*, 2003, **11**, 9–15.
- 15 K. Malinowski, M. Ebisz, R. F. LaPrade and M. Mostowy, *Appl. Sci.*, 2021, **11**, 3993.
- 16 A. T. Hexter, T. Thangarajah, G. Blunn and F. S. Haddad, *Bone Joint J.*, 2018, **100-B**, 271–284.
- 17 H. Mutsuzaki, T. Kinugasa and M. Sakane, *J. Orthop.*, 2019, **16**, 422–425.
- 18 A. P. Duarte, J. F. Coelho, J. C. Bordado, M. T. Cidade and M. H. Gil, *Prog. Polym. Sci.*, 2012, **37**, 1031–1050.
- 19 J. Guo, W. Sun, J. P. Kim, X. Lu, Q. Li, M. Lin, O. Mrowczynski, E. B. Rizk, J. Cheng, G. Qian and J. Yang, *Acta Biomater.*, 2018, **72**, 35–44.

- 20 J. Guo, G. B. Kim, D. Shan, J. P. Kim, J. Hu, W. Wang, F. G. Hamad, G. Qian, E. B. Rizk and J. Yang, *Biomaterials*, 2017, **112**, 275–286.
- 21 Z. Qiao, X. Lv, S. He, S. Bai, X. Liu, L. Hou, J. He, D. Tong, R. Ruan, J. Zhang, J. Ding and H. Yang, *Bioact. Mater.*, 2021, **6**, 2829–2840.
- 22 X. Pei, H. Zhang, Y. Zhou, L. Zhou and J. Fu, *Mater. Horiz.*, 2020, **7**, 1872–1882.
- 23 T. Xie, J. Ding, X. Han, H. Jia, Y. Yang, S. Liang, W. Wang, W. Liu and W. Wang, *Mater. Horiz.*, 2020, **7**, 605–614.
- 24 X. Lu, S. Shi, H. Li, E. Gerhard, Z. Lu, X. Tan, W. Li, K. M. Rahn, D. Xie, G. Xu, F. Zou, X. Bai, J. Guo and J. Yang, *Biomaterials*, 2020, **232**, 119719.
- 25 J. Guo, W. Wang, J. Hu, D. Xie, E. Gerhard, M. Nisic, D. Shan, G. Qian, S. Zheng and J. Yang, *Biomaterials*, 2016, **85**, 204–217.
- 26 J. Guo, X. Tian, D. Xie, K. Rahn, E. Gerhard, M. L. Kuzma, D. Zhou, C. Dong, X. Bai, Z. Lu and J. Yang, *Adv. Funct. Mater.*, 2020, **30**, 2002438.
- 27 Z. Qiao, X. Lv, S. He, S. Bai, X. Liu, L. Hou, J. He, D. Tong, R. Ruan, J. Zhang, J. Ding and H. Yang, *Bioact. Mater.*, 2021, **6**, 2829–2840.
- 28 D. Xie, J. Guo, M. R. Mehdizadeh, R. T. Tran, R. Chen, D. Sun, G. Qian, D. Jin, X. Bai and J. Yang, *J. Mater. Chem. B*, 2015, **3**, 387–398.
- 29 E. Davies, K. H. Muller, W. C. Wong, C. J. Pickard, D. G. Reid, J. N. Skepper and M. J. Duer, *Proc. Natl. Acad. Sci. U. S. A.*, 2014, **111**, E1354–E1363.
- 30 C. Ma, X. Tian, J. P. Kim, D. Xie, X. Ao, D. Shan, Q. Lin, M. R. Hudock, X. Bai and J. Yang, *Proc. Natl. Acad. Sci. U. S. A.*, 2018, **115**, E11741–E11750.
- 31 U. Grober, J. Schmidt and K. Kisters, *Nutrients*, 2015, **7**, 8199–8226.
- 32 J. L. Wang, J. K. Xu, C. Hopkins, D. H. Chow and L. Qin, *Adv. Sci.*, 2020, **7**, 1902443.
- 33 Y. Zhang, J. Xu, Y. C. Ruan, M. K. Yu, M. O’Laughlin, H. Wise, D. Chen, L. Tian, D. Shi, J. Wang, S. Chen, J. Q. Feng, D. H. K. Chow, X. Xie, L. Zheng, L. Huang, S. Huang, K. Leung, N. Lu, L. Zhao, H. Li, D. Zhao, X. Guo, K. Chan, F. Witte, H. C. Chan, Y. Zheng and L. Qin, *Nat. Med.*, 2016, **22**, 1160–1169.
- 34 J. Wang, J. Xu, B. Song, D. H. Chow, P. Shu-Hang Yung and L. Qin, *Acta Biomater.*, 2017, **63**, 393–410.
- 35 J. Wang, Y. Wu, H. Li, Y. Liu, X. Bai, W. Chau, Y. Zheng and L. Qin, *Biomaterials*, 2018, **157**, 86–97.
- 36 H. L. Jang, K. Jin, J. Lee, Y. Kim, S. H. Nahm, K. S. Hong and K. T. Nam, *ACS Nano*, 2019, **8**, 634–641.
- 37 H. D. Kim, H. L. Jang, H.-Y. Ahn, H. K. Lee, J. Park, E. Lee, E. A. Lee, Y. H. Jeong, D.-G. Kim, K. T. Nam and N. S. Hwang, *Biomaterials*, 2017, **112**, 31–43.
- 38 F. A. Shah, B. E. J. Lee, J. Tedesco, C. L. Wexell, C. Persson, P. Thomsen, K. Grandfield and A. Palmquist, *Nano Lett.*, 2017, **17**, 6210–6216.
- 39 S. P. Sevari, J. K. Kim, C. Chen, A. Nasajpour, C.-Y. Wang, P. H. Krebsbach, A. Khademhosseini, S. Ansari, P. S. Weiss and A. Moshaverinia, *ACS Appl. Mater. Interfaces*, 2021, **13**, 35342–35355.
- 40 S. Singh, J. Dodt, P. Volkers, E. Hethershaw, H. Philippou, V. Ivaskevicius, D. Imhof, J. Oldenburg and A. Biswas, *Sci. Rep.*, 2019, **9**, 11324.
- 41 M. Mehdizadeh, H. Weng, D. Gyawali, L. Tang and J. Yang, *Biomaterials*, 2012, **33**, 7972–7983.